PAPER

Composite hydrogels of polyacrylamide and crosslinked pH-responsive micrometer-sized hollow particles†

Kyriaki Pafiti,[a] Zhengxing Cui,[a] Louise Carney,[a] Anthony J. Freemont[b] and Brian R. Saunders*[a]

Whilst hydrogels and hollow particles both continue to attract much attention in the literature there are few examples of hydrogel composites containing hollow particles. Here, we study composite polyacrylamide (PAAm) hydrogels containing micrometer-sized pH-responsive shell-crosslinked hollow particles (abbreviated as HP_{XL}) based on poly(methylmethacrylate-*co*-methacrylic acid) functionalised with glycidyl methacrylate (GMA). The HP_{XL} particles were prepared using our scaleable emulsion template method and inclusion of GMA was found to promote spherical hollow particle formation. The pendant vinyl groups from GMA enabled shell-crosslinked hollow particles to be prepared prior to formation of the PAAm/HP_{XL} composite gels. The morphologies of the particles and composite gels were studied by optical microscopy, confocal laser scanning microscopy and scanning electron microscopy. Dynamic rheology measurements for the composite gels showed that the modulus variation with HP_{XL} concentration could be described by a percolation model with a HP_{XL} percolation threshold concentration of 4.4 wt% and a scaling exponent of 2.6. The composite gels were pH-responsive and largely maintained their mechanical properties over the pH range 4.0 to 8.0. Because the composite gels had tuneable mechanical properties (with modulus values up to 530 kPa) and were pH-responsive they are potential candidates for future wound healing or membrane applications.

Introduction

Hydrogels have attracted considerable interest in the biomedical field,[1] including drug[1,2]/gene delivery, stem cell and cancer research, cell therapy[3] and regenerative medicine[4] due to their tuneable structural, compositional and mechanical properties. Both naturally-derived hydrogels and synthetic hydrogels have been used widely in regenerative medicine due to their favourable biocompatibilities and mechanical property similarities with native tissues.[4,5] Reinforcement strategies have been used to improve gel mechanical properties, which include the development of double networks.[6–8] Workers have also investigated composite hydrogels containing inorganic nanoparticles. These nanocomposite gels combine high modulus, which is associated with the high surface area of the nanoparticles, with high extensibility.[9–14] Nanocomposite gels have been prepared *via* incorporation of different species;[15] these include mineral (organic or inorganic clays),[16] metallic (gold and silver[17] nanoparticles), magnetic[18] (iron or gadolinium) and carbon-based (graphene oxide[19,20] or carbon nanotubes[21]) species. Much less work has been reported for hydrogel composites containing micrometer-sized hollow particles, which is the focus of this study. We hypothesised that micrometer-sized particles would enable formation of composite gels containing high hollow particle concentrations without excessively large modulus values because of the low surface area-to-volume ratios of the particles. The pH-responsive micrometer-sized hollow particles used here offer potential to include larger sized species (*e.g.*, proteins or cells) within composite gels and may provide new opportunities for triggered release of biological species.

Hollow nano- and micrometer-sized spherical particles are of great technological importance because of their potential encapsulation utility in cosmetics, corrosion protection,[22] paper coatings, delivery[23] and as protective shells.[24,25] For the preparation of hollow particles emulsion processing,[26–28] multi-layer assembly[29,30] and colloid templating methods (mainly based on silica particles)[31,32] have been most commonly used. Here, we focus on the use of pH-responsive micrometer-sized hollow particles in order to investigate the effects they have on composite hydrogel morphological and mechanical properties. In this study the hollow

[a] Biomaterials Research Group, School of Materials, The University of Manchester, MSS Tower, Manchester, M13 9PL, UK. E-mail: brian.saunders@manchester.ac.uk

[b] Division of Regenerative Medicine, School of Medicine, Stopford Building, The University of Manchester, Oxford Road, Manchester, M13 9PT, UK

† Electronic supplementary information (ESI) available. See DOI: 10.1039/c5sm02521d

particle structure and intra-shell crosslinking were controlled by including vinyl functionality within the hollow particle shells and crosslinking these groups (later).

Our hollow particles were prepared using a simple, scaleable, emulsion templating method that was facilitated by the amphiphilic nature of the pH-responsive vinyl-functionalised poly(methylmethacrylate-co-methacrylic acid) (PMMA-MAA) copolymer and its migration to the dichloromethane/water interface.[33] The hollow particles studied here, which are pH responsive, differ considerably to the thermally responsive hollow poly(N-isopropyacrylamide)-based microgel particles reported elsewhere.[34–36] In contrast to earlier work which focussed on dispersions and physical gels of hollow particles,[37,38] here a study of poly(acrylamide) (PAAm) composite gels containing shell-crosslinked pH-responsive hollow particles is presented for the first time. After characterising the new hollow particles we investigate the morphology and mechanical properties of composite hydrogels. Inclusion of the hollow particles increased the composite gel modulus values and the data were successfully modelled using a percolation model. The mechanisms responsible for the mechanical properties of these new composites are discussed. We show that the composite gels are pH-responsive over the pH range of 4.0 to 8.0. The new composite hollow particle gels presented here may have potential applications as wound dressings or membranes.

Experimental section

Materials

Unless stated otherwise all materials were purchased from Sigma-Aldrich and used as received. The monomers used were methyl methacrylate (MMA, 99%), tert-butyl methacrylate (t-BuMA, 98%), glycidyl methacrylate (GMA, 97%), AAm ($\geq$98%) and N,N'-methylene bisacrylamide (MBAAm, 99%). t-BMA and MMA contained 200 ppm and less than 30 ppm of inhibitor, respectively, based on supplier information. A preliminary study showed that the presence of the inhibitors did not have a discernible effect on copolymer and hollow particle properties and consequently the monomers were used without inhibitor removal. Azoisobutyronitrile (AIBN, 99%) was purchased from VWR. The other reagents and initiators were triphenylphosphine (99%), ammonium persulfate (APS, $\geq$98%) and N,N,N',N'-tetramethylethylenediamine (TEMED, 99%), 2-hydroxy-1-(4-(2-hydroxyethoxy)phenyl)-2-methyl-propan-1-one (98%, photoinitiator) and 2,2-diphenyl-1-picryl-hydrazyl (DPPH). The chromophore used was Rhodamine B. The stabiliser employed was poly(vinyl pyrolidone) (PVP) with average molecular weight of 40 000 g mol^{-1}. The solvents used were tetrahydrofuran (THF, anhydrous, $\geq$99%), dimethyl-formamide (DMF, anhydrous, $\geq$99.8%), methanol (reagent grade), diethyl ether (reagent grade) and dichloromethane (DCM, reagent grade). All water used for this study was distilled and deionised. The copolymers employed to prepare the hollow particles are listed in Table 1 and the methods used for their synthesis are described in the ESI.† Note that in this work the MAA units within the copolymers were prepared by hydrolysis of copolymerised t-BMA units within PMMA-t-BuMA as described in Scheme S1 (ESI†).

Hollow particle and composite gel identification

Three types of hollow particles and composite gels were studied and are identified in Table 1. The preparation methods for the hollow particles containing unreacted vinyl groups from GMA (abbreviated as HP$_{VF}$) and shell-crosslinked hollow particles (abbreviated as HP$_{XL}$) are depicted in Scheme 1. All hollow particles were prepared at 0 °C. Hollow particles that did not contain GMA groups (abbreviated as HP) were prepared using the same method as used to prepared HP$_{VF}$. All PAAm/hollow particle gels were prepared using AAm (12 wt%) and MBAAm (1 wt%). The composite gels are identified as PAAm/HP$_{XL(y)}$, PAAm/HP$_{VF(y)}$ and PAAm/HP$_{(y)}$ where the values for y represent the hollow particle concentration used for gel preparation (in wt%). As an example, PAAm/HP$_{XL(10)}$ represents a composite gel prepared using AAm (12 wt%), MBAAm (1 wt%) and HP$_{XL}$ (10 wt%).

Preparation of non-GMA functionalised hollow particles

HP dispersion preparation was performed using a similar emulsion templating method as reported previously.[37] Briefly, PMMA-MAA (1.0 g) was dissolved in a cosolvent blend (22 mL) of DCM and methanol solvents (volume ratio, 8.4:1.6). The polymer solution was added into a PVP solution (60 mL, 4% w/w) over a constant rate of 10 mL min^{-1} which was sheared at 10 000 rpm using a Silverson LR4 high speed mixer with cooling (0 °C). The emulsification continued for 30 s after polymer solution addition was complete. Afterwards, the emulsion was allowed to stir gently overnight to enable removal of DCM. Finally, the product was purified by repeated centrifugation and redispersion in water in order to remove excess PVP, followed by filtration using a 50 μm filter. The purified HP dispersion was dried in vacuum at room temperature.

## Preparation of vinyl functionalised hollow particles

The preparation of HP$_{VF}$ was performed using PMMA-MAA$_{0.20}$-GMA$_{0.12}$ and followed the same procedure described above for the HP dispersion.

Table 1 Identities and compositions of copolymers, hollow particles and composite gels

Hollow particle	Copolymer composition[a]	mol% MAA[a]	Hollow particle details	Composite gel[b]
HP$_{XL}$	PMMA-MAA$_{0.20}$-GMA$_{0.12}$	20	Shell-crosslinked hollow particles vinyl functionalised with GMA.	PAAm/HP$_{XL(y)}$
HP$_{VF}$	PMMA-MAA$_{0.20}$-GMA$_{0.12}$	20	Unreacted GMA groups present in hollow particles	PAAm/HP$_{VF(y)}$
HP	PMMA-MAA$_{0.35}$	35	Hollow particles that were not functionalised with GMA	PAAm/HP$_{(y)}$

[a] Compositions determined by ^{1}H NMR spectroscopy (see ESI). [b] The values of y is the concentration of hollow particles (wt%) used for composite gel preparation. All gels studied were prepared using 12 wt% AAm and 1 wt% of MBAAm.
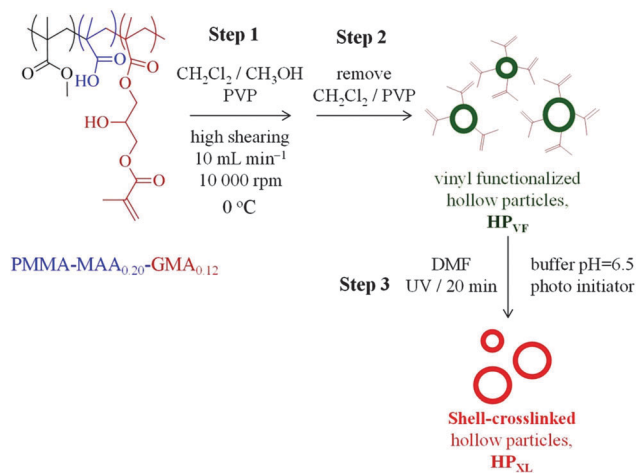
Scheme 1 Hollow particle preparation. Depiction of preparation of hollow particles containing unreacted vinyl groups (HP$_{VF}$) and shell-crosslinked hollow particles (HP$_{XL}$). Hollow particles that did not contain pendant vinyl groups (HP) were also prepared. In that case PMMA-MAA$_{0.35}$ was used as well as steps 1 and 2.

Preparation of shell-crosslinked hollow particles

To prepare HP$_{XL}$, the appropriate mass of HP$_{VF}$ particles was dispersed in buffer solution at pH 6.4 to give a HP$_{VF}$ concentration of 30 wt%, followed by the addition of the photoinitiator (3 wt%). To the polymer mixture a small amount of DMF was added to give a volume fraction of 10 vol%. Then, the mixture was sealed with a sheet of polypropylene to prevent evaporation and UV-irradiated for 30 min at 254 nm using a UV Crosslinker (Ultra-violet Products Ltd).

Preparation of composite hydrogels

HP, HP$_{VF}$ and HP$_{XL}$ were used to prepare three series of PAAM composite hydrogels (see Table 1). The preparation of PAAm/HP$_{XL(20)}$ is described as an example. AAm (0.36 g, 5.06 mmol) and MBAAm (0.030 g, 0.19 mmol) were added to a dispersion (2.0 ml) containing HP$_{XL}$ (0.60 g) and stirred for 5.0 min. Water was added to adjust the final HP$_{XL}$ concentration to 20 wt%. APS (18.0 µL, 7.89 µmol) and TEMED (4.5 µL, 30 µmol) were added and the mixture purged with N$_2$. The dispersion was heated at 60 °C until gelation occurred. The latter temperature was used in order to decrease the time for gelation and prevent significant hollow particle sedimentation. All the other composite gels were prepared using a similar method using the proper masses of HP$_{XL}$, HP$_{VF}$ or HP. The pH of the composite gels studied in this work was ~6.0 unless otherwise stated.

Characterisation techniques

PMMA-t-BuMA copolymer was analysed using a GPC system equipped with a Shodex RI-101B refractive index detector at 35 °C. The mobile phase was THF, delivered at a flow rate of 1 mL min^{-1}. The molecular weights were based on linear PMMA standards. The sample was dissolved in THF (0.2% w/v) and filtered prior to injection. The ^{1}H NMR spectra of PMMA-t-BuMA (in CDCl$_3$) as well as those of PMMA-MAA before and after vinyl functionalisation were obtained using a Bruker 400 MHz instrument (Fig. S1, ESI†). Potentiometric titration of the copolymers (1 wt% dispersion) was performed using a Mettler Toledo titration unit using NaOH (1.0 M).

HP$_{VF}$ and HP$_{VF-XL}$ (0.1% w/w dispersion) optical images were obtained using an Olympus BX41 microscope and white transmitted light. Confocal laser scanning microscopy (CLSM) images were conducted using a Leica TCS SP5 broadband confocal instrument and Rhodamine B was used as the chromophore. A few drops of aqueous Rhodamine B solution (1 wt%) were mixed with the hollow particle dispersions and left for 24 h before obtaining CLSM images. The excitation wavelength used was 552 nm. SEM images of the freeze-dried gels (using liquid N$_2$) were obtained using a Philips XL30 FEG SEM instrument. Dispersions of particles (10^{-5} wt%) were deposited on SEM stubs by evaporation at room temperature. The measurement of hollow particle size was performed using the Image J software. For rheology measurements a TA Instruments AR G2 temperature controlled rheometer which was equipped with an environmental chamber was used. For all gels a plate geometry (20 mm diameter) was employed. For measurements, the frequency sweep data were varied from 0.1 to 100 Hz, while the strain sweep data were run between 0.1 and 200%.

The composite gels were also characterised in terms of their degrees of swelling (DS) at pH values of 4.0 and 8.0. Two or three samples from each composite gel (approximate dimensions of 1.5 cm × 0.5 cm × 0.3 cm) were placed in small vials and were dried in a vacuum oven at room temperature for 72 h. Subsequently, aqueous buffer solutions at pH 4.0 and 8.0 (6.0 mL) were added to vials, and the hydrogels were left to swell. The buffers contained potassium dihydrogen phosphate and borax, respectively, and had nominal ionic strengths of 0.1 M. Periodically, the samples were reweighed (after carefully removing surface water) to determine their swollen mass. The DS values reported here were obtained after a swelling duration of 14 days. The DS values were calculated as the ratio of the average swollen network mass divided by the dry network mass determined gravimetrically.

Results and discussion

Synthesis and characterisation of hollow particles

The synthesis and characterisation of the copolymers used to prepare the hollow particles are described in the ESI.† Their compositions are shown in Table 1. The latter were obtained from ^{1}H spectra (see Fig. S1, ESI†). The scaleable hollow particle preparation method used was straightforward and based on our earlier work.[33,34] PMMA-MAA$_{0.20}$-GMA$_{0.12}$ was used for the preparation of hollow particles containing unreacted vinyl groups (HP$_{VF}$) and also shell-crosslinked particles (HP$_{XL}$). As a control system, PMMA-MAA$_{0.35}$ was used to prepare non-GMA functionalised hollow particles (HP).

The HP$_{XL}$ and HP$_{VF}$ hollow particles have not been previously reported. Potentiometric titration data for HP and HP$_{VF}$ dispersions were measured (Fig. S2, ESI†). The apparent pK_a

was determined from the pH corresponding to half the volume of NaOH added at the stoichiometric point. The latter and the mass of particles present were used to calculate the MAA content. The apparent pK_a for the HP particles was 7.0 and the MAA content found by this method was 36.5 mol% The HP_{VF} particle titration data gave an apparent pK_a of 8.5 and the MAA and GMA contents determined from the data were 21.0 and 15.5 mol%, respectively. There was also a pH maximum when the neutralisation was ∼10 mol%. Related pH maxima were reported earlier for PMMA-MAA containing ∼20 mol% MAA and was attributed to a combination of pH-triggered shell expansion and subsequent pH buffering.[39] The relatively high apparent pK_a value for the HP_{VF} particles is due to their lower MAA content. The MAA contents determined from the titration data for both HP and HP_{VF} were within 1.5 mol% of the respective values determined using ^{1}H NMR spectroscopy (Table 1), which shows that all of the MAA groups were accessible to OH^-.

The morphologies of HP_{XL}, HP_{VF} and HP particles were probed using optical microscopy, CLSM and SEM. Optical microscopy (Fig. 1a, d and g) and CLSM images (Fig. 1b, e and h) of the HP_{XL} and HP_{VF} dispersions in water revealed spherical hollow particles. As noted earlier[40] the HP dispersions contained hollow particles that were deformed (Fig. 1g and h). For all three systems the particles were polydisperse due to the turbulent flow present during the high shear emulsification method used to prepare the particles.

Analysis of the SEM images (Fig. 1c, f and i) gave number-average diameters for HP_{XL} and HP_{VF} of 4.2 ± 2.6 and 3.6 ± 1.8 μm, respectively, and they were not significantly different.

In the case of HP the average equivalent spherical diameter was 4.4 ± 1.4 μm. CLSM images (Fig. 1b, e and h) indicate shell thicknesses in the range 1–2 μm. The SEM images of fragmented (Fig. 1c, inset) or folded (Fig. 1f, inset) hollow particles are consistent with this range. The average shell thickness can be estimated as ∼20% of the hollow particle diameter.

A new finding from this study is that the GMA functionalisation of the parent PMMA-MAA copolymer improved the spherical morphology of the hollow particles as can be seen by comparison of the SEM images for HP_{XL} (Fig. 1c), HP_{VF} (Fig. 1f) and the GMA-free HP system (Fig. 1i). We propose that GMA increased the hydrophobicity and decreased the total extent of hydrogen bonding between RCOOH groups during solvent evaporation and shell formation. Both factors should have favoured conformational rearrangement during phase separation and promoted the development of a smoother shell.

Composite gel morphology

HP_{XL}, HP_{VF} and HP were used for the preparation of the composite gels, PAAm/$HP_{XL(y)}$, PAAm/$HP_{VF(y)}$ and PAAm/$HP_{(y)}$, respectively (See Table 1 and Scheme 2). The latter two systems were used as controls to help elucidate the effects of HP_{XL} shell crosslinking for the PAAm/$HP_{XL(y)}$ gels. Whilst HP_{VF} contained unreacted GMA groups, the conditions used for preparation of the control PAAm/$HP_{VF(y)}$ gel (*i.e.*, hydrophilic APS and pH much less than the pK_a) deliberately favoured reaction of surface GMA groups for HP_{VF} with the growing PAAm network and not the buried GMA groups.
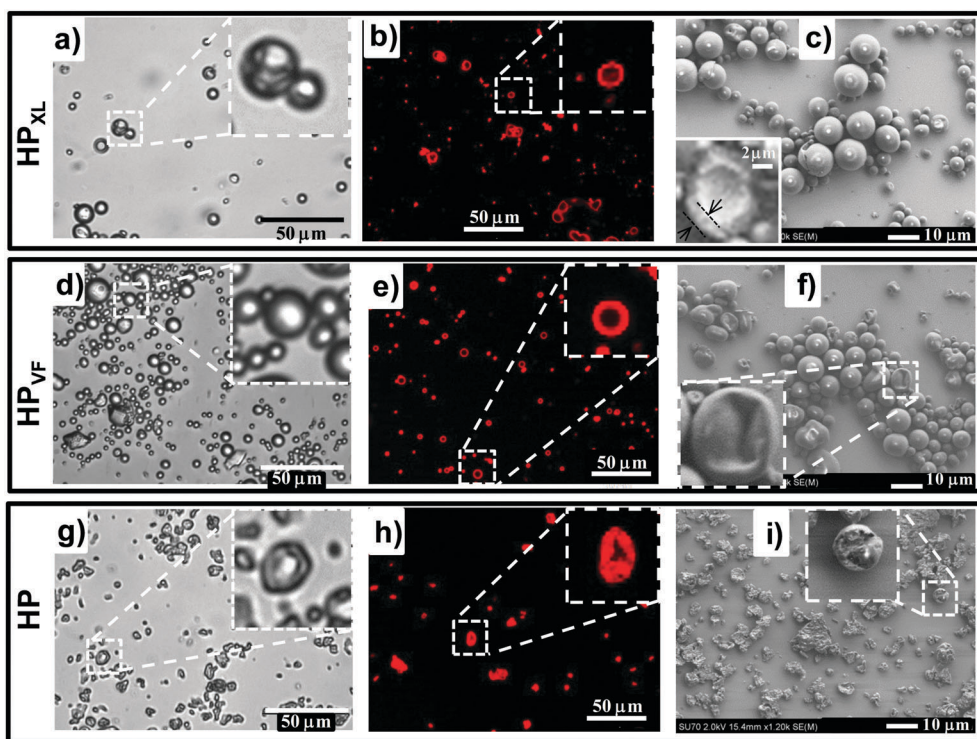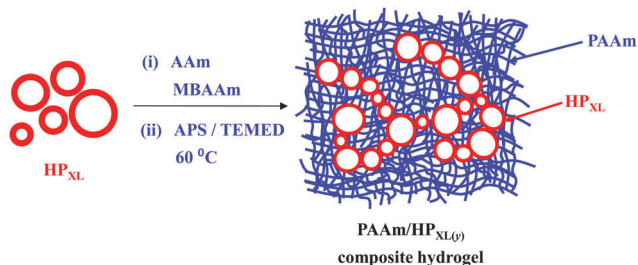

Fig. 1 Hollow particle morphologies. The identities of the hollow particles are shown in the left hand side of each row. Images from optical microscopy (left hand column) as well as CLSM (middle column) and SEM (right hand column) are shown. The pH of the dispersions was ∼5.6 for all systems.

Scheme 2 Composite gel preparation. Depiction of the procedure used for the preparation of PAAm/HP$_{XL(y)}$ composite gels. The same method was also used for the preparation of PAAm/HP$_{VF(y)}$ and PAAm/HP$_{(y)}$ gels.

The composite gels formed free-standing gels (inset of Fig. 2h) and the morphologies of the composite gels were investigated using CLSM and SEM. Fig. 2a shows an CLSM image for PAAm/HP$_{XL(10)}$ and hollow particles are clearly evident

and confirm that the hollow particles remained intact during PAAm network growth. SEM images of freeze-dried gel samples (Fig. 2b and c) show hollow particle cross sections. The hollow particles (arrows) had thick shells and may have fractured due to thermal stresses present during freeze-drying. CLSM images for PAAm/HP$_{VF(20)}$ gels (Fig. 2d) also showed spherical hollow particles which were also evident from SEM images (Fig. 2e and f). Whilst the PAAm/HP$_{(20)}$ gel also contained hollow particles (Fig. 2g), the particles were deformed, which was also apparent from the SEM images for PAAm/HP$_{(10)}$ (Fig. 2h and i).

The SEM images for PAAm are also shown for comparison (Fig. 2j and k). The morphology is similar to that commonly reported for AAm hydrogels and consisted of micrometer-sized pores that formed as a consequence of freeze-drying.[41] In the hydrated state the pores would have contained expanded PAAm chains. This porous morphology can be seen from the SEM images for each of the composite gels (Fig. 2). Consequently, we
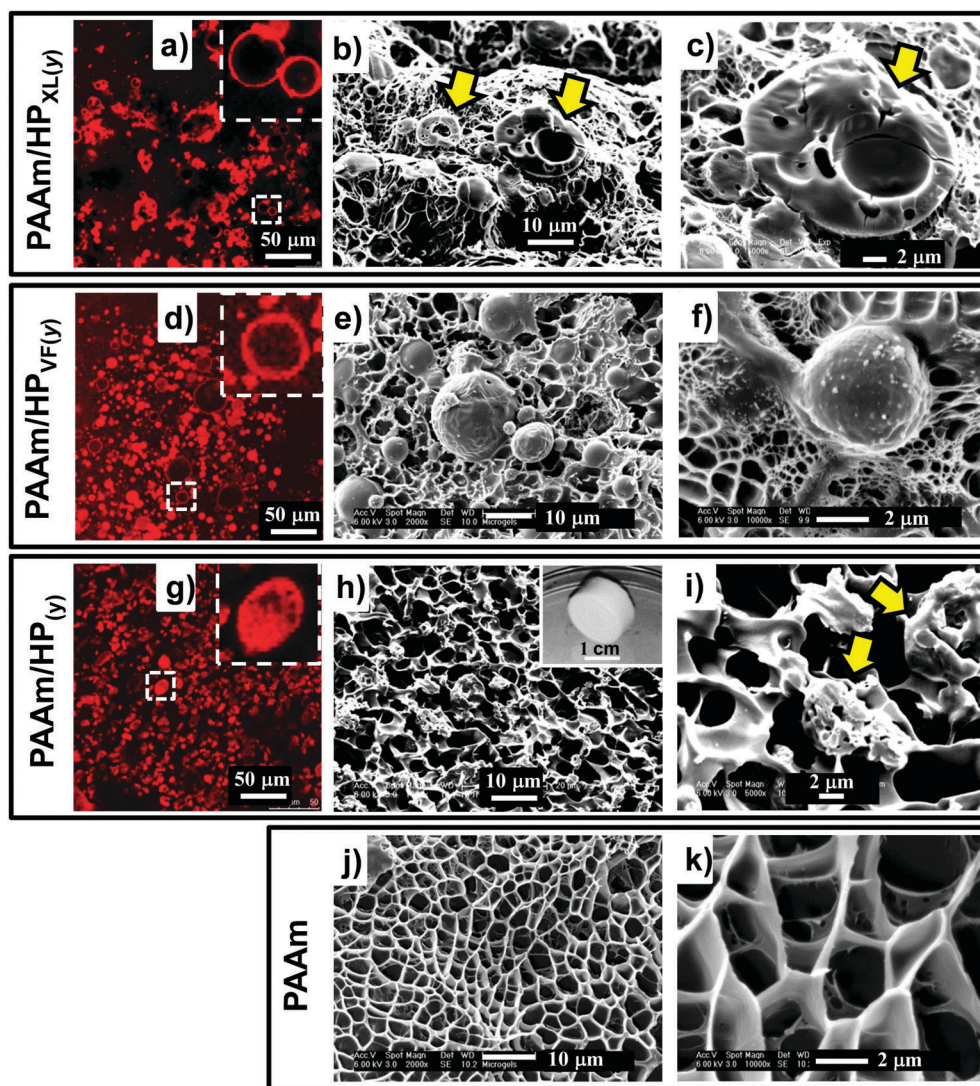

Fig. 2 Composite gel morphologies. The identities of the gels are shown on the left hand side of each row. CLSM images are shown in (a), (d) and (g). The remaining images are from SEM of freeze-dried samples. The inset of (h) shows a free-standing gel. The values of y for all of the composite gels were 10 with the exception of (d) and (g), where the y values were 20. The arrows in (b), (c) and (i) identify hollow particles.

conclude that the composite PAAm/hollow particle composite gel morphologies were combinations of those for PAAm gel (Fig. 2j and k) and the respective hollow particles (Fig. 1).

Composite gel mechanical properties

The composite gels studied here are unusual compared to most reported gel composites[42,43] because of the high (hollow) particle concentrations present and the relatively large size of the hollow particles. The mechanical properties of the PAAm/HP$_{XL(y)}$ gels were studied using dynamic rheology. For this study PAAm/HP$_{VF(y)}$, PAAm/HP$_{(y)}$ and PAAm gel were used as controls. The frequency dependence of the storage modulus (G') (Fig. 3a, c and e) increased with increasing hollow particle concentration (y). By contrast the G' data for the PAAm gel ($y = 0$) had negligible frequency dependence. Fig. 3 also shows $\tan\delta(=G''/G'$, where G'' is the loss modulus) *versus* frequency data (Fig. 3b, d and f). The PAAm gel ($y = 0$) had $\tan\delta$ values that were independent of frequency (Fig. 3b) indicating an ideal elastic response for the network.[44] The frequency dependences of $\tan\delta$ for PAAm/HP$_{XL(y)}$ ($y = 2$–20%) were also low (Fig. 3b). However, a pronounced frequency dependence was evident at the highest hollow particle concentration ($y \geq 25\%$) for all composite gels (Fig. 3b, d and f). It follows that for the composite gels with $y \leq 20\%$ the PAAm network was able to accommodate the hollow particles without significant disruption of the PAAm network. At higher y values the elastic response was no longer ideal which is likely due

to the dominance of the particle–particle network for stress distribution.

The average G' and $\tan\delta$ values from the frequency-sweep data (corresponding to a frequency of ~ 1.6 Hz) are shown as function of y in Fig. 4. The most striking feature of the data is the major increases of both G' (Fig. 4a) and $\tan\delta$ (Fig. 4b) that occur once y increases beyond 5%. The increase of $\tan\delta$ with y (Fig. 4b) shows that the inclusion of hollow particles introduced additional inelastic deformation pathways within the composite gels and these were most pronounced for the PAAm/HP$_{XL}$ gels. A potential source of inelastic deformation is the relative movement of hollow particles under strain. Because the HP$_{XL}$ particles were exclusively shell-crosslinked one can imagine less efficient encapsulation of the HP$_{XL}$ particles near to the particle/PAAm interface and a greater chance for inelastic displacement.

What is the mechanism responsible for the variation of G' with hollow particle concentration for the PAAm/HP$_{XL}$ gels shown in Fig. 4a? Supra-linear behaviour of the modulus with particle concentration is often observed for nanocomposite gels.[45] The two primary mechanisms for modulus reinforcement for nanocomposite gels are interfacial interactions or percolation of the particles.[46] Interfacial interactions are important for nanocomposite gels[45] due to the high surface area-to-volume ratio of the nanoparticles. If we assume an average hollow particle diameter of ~ 4 μm and that PAAm chains within 200 nm of the HP interface were constrained by contacts
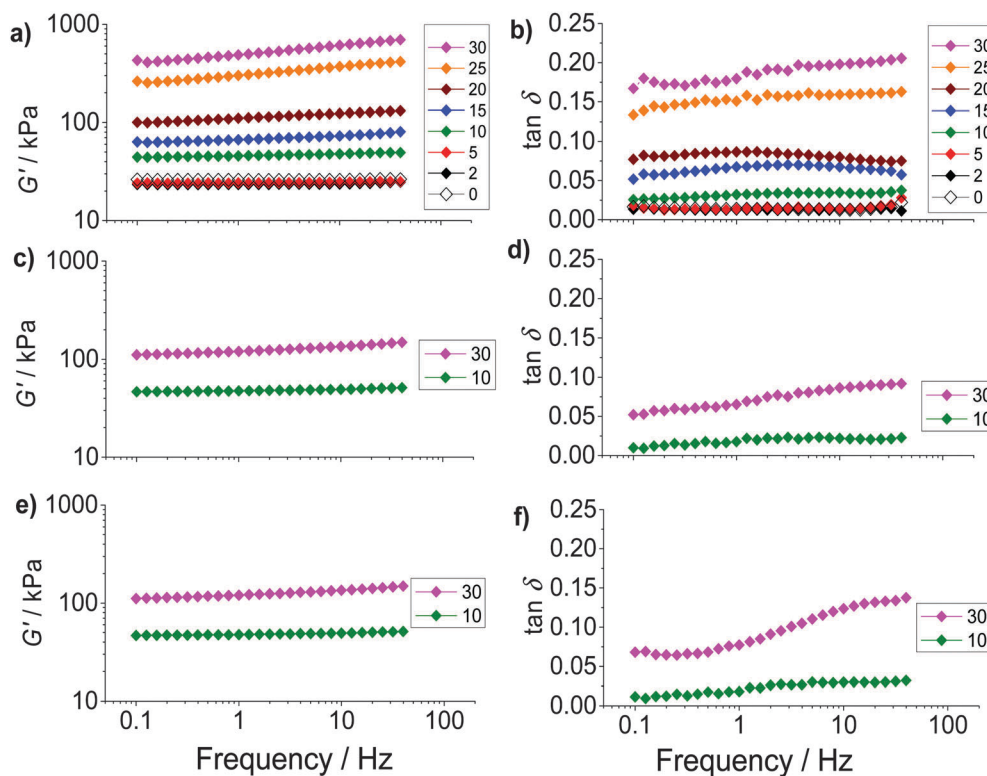

Fig. 3 Frequency-sweep rheology study. The variations of G' (storage modulus) and $\tan\delta(=G''/G'$, where G'' is the loss modulus) with frequency are shown in the left and right columns, respectively, for PAAm/HP$_{XL(y)}$ (a and b), PAAm/HP$_{VF(y)}$ (c and d) and PAAm/HP$_{(y)}$ (e and f). The legends show the values for y (%).
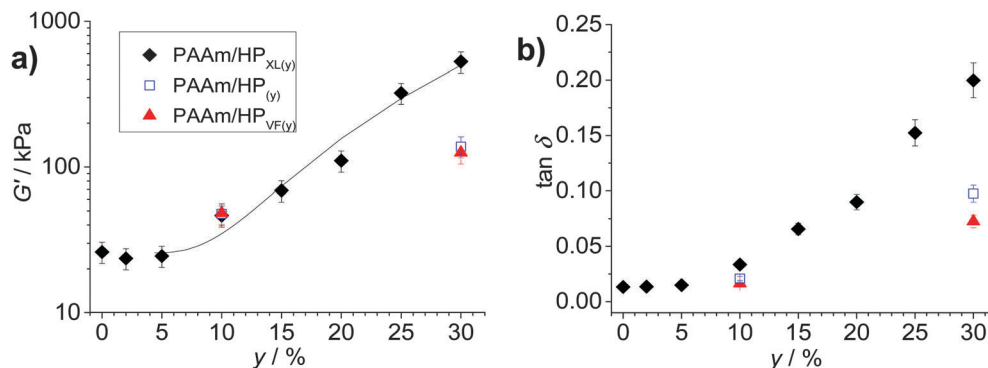
Fig. 4 Effects of hollow particle concentration on gel mechanical properties. The variations of (a) G' and (b) $\tan\delta$ with particle concentration (y) are shown for the three composite gels. The data have been taken from Fig. 3. The legend applies to both graphs. The curve in (a) is the fit from eqn (1). The value for A was 0.10.

with the interface, which restricted their conformations,[47] it can be shown that for PAAm/HP$_{XL(20)}$ less than 1% of the PAAm chains could have been affected by the hollow particle interfaces. By contrast hydrogels containing 18 nm silica nanoparticles had a maximum of about 40% of their chains adsorbed to the silica interface.[48] Hence, interfacial interactions are not considered to have been significant for our PAAm/hollow particle gels. It was the use of low surface area-to-volume ratio micrometer-sized hollow particles that was hypothesised to enable high y values to be achieved without producing highly stiff, brittle, gels. The range of G' values achieved for the gels (40–530 kPa) is wide (but not excessively high) and covers modulus values corresponding to skin[49] and other soft tissue, which includes heart tissue.[50]

In order to test for percolation we applied the following equation which is an extension of particulate gel percolation models from van der Linden and Sagis[51] and Mitsumata *et al.*[52]

$$G' = G_{m}' + A(y - y_{c})^{n} \qquad (1)$$

For eqn (1), G_{m}', A, y_{c} and n are the matrix modulus, a constant, the particle percolation threshold concentration and the scaling exponent, respectively. The parameter G_{m}' takes into account the finite modulus for PAAm that was present in the absence of hollow particles ($y = 0$). Inspired by the method of van der Linden and Sagis[51] we plotted $(\Delta G')^{1/n}$ (where $\Delta G' = G' - G_{m}'$) as a function of y (see Fig. S3, ESI†). The line of best fit chosen had the maximum R^2 value (Fig. S4, ESI†) and was obtained when $n = 2.6$. The corresponding value for $y_{c}(= -\text{intercept/gradient})$ was 4.4%. The good fit to the data is support for (hollow particle) percolation applying for PAAM/HP$_{XL(y)}$. The n value of 2.6 is comparable to that reported for other systems[53] and is the range that is typical for inhomogenous systems.[51]

We next briefly consider the control gels. Whilst there is no significant difference between the G' values for the PAAm/HP$_{XL(y)}$ data compared to those for the control samples when $y = 10\%$ (Fig. 4a), major differences were apparent for $y = 30\%$. For those systems the G' values decreased in the order: PAAm/HP$_{XL(30)} \gg$ PAAm/HP$_{(30)} >$ PAAm/HP$_{VF(30)}$. We attribute the higher modulus for the former to shell-crosslinking for PAAm/HP$_{XL}$, which increased the hollow particle modulus and hence the contribution

of the hollow particle network to the overall gel modulus. The relatively low modulus values for PAAm/HP$_{VF(30)}$ and PAAm/HP$_{(30)}$ are ascribed to a lack (or absence) of intra-shell crosslinking. Another control composite PAAM/HP$_{20}$ gel was also prepared which did not contain added MBAAm. The composite had a very low modulus (2.3 kPa), high $\tan\delta$ value (0.84) at a frequency of 1.6 Hz and inelastically deformed when strained. Consequently, the composite gel had poor mechanical stability. Therefore, the roles of MBAAm were to increase matrix crosslinking (and matrix modulus) and composite mechanical stability.

To probe ductility and dissipation strain-sweep data were also obtained (Fig. 5). All of the composite gels showed linear viscoelastic regions for strain values less than ~10%. The G' values (Fig. 5a) decreased at higher strain values due to the onset of network breakdown. Fig. 5b shows the variation of G'' with strain for PAAm/HP$_{XL(y)}$. The data show clearly that inclusion of the hollow particles strongly increased the G'' values (and energy dissipation) at low strain (indicated by the arrow). A maximum was present at high strain for PAAm ($y = 0$), as well as for the composite gels, which is attributed to PAAm network breakdown. We propose that at low strain (*e.g.*, ~0.2–1.0%) the hollow particles consumed strain energy by deformation, fracture and inelastic particle movement. The latter probably included hollow particle-to-hollow particle bond breaking. At high strain (*e.g.*, ~20–70%) the PAAm network dissipated energy through strand breakage and network breakdown. As y increased the dissipation changed from being dominated by the PAAm network (*e.g.*, $y < 5\%$) to having a large contribution from the percolated hollow particle network (*e.g.*, $y \geq 10\%$).

The strain dependence for G'' is shown for PAAm/HP$_{VF(y)}$ and PAAm/HP$_{(y)}$ in Fig. 5d and f, respectively. Once again, the increase in the G'' values at low strain can be seen as y increased. The extent of energy dissipation at low strain as evidenced by G'' was about a factor of 10 lower when $y = 30\%$ for these two composite gels compared to that for PAAm/HP$_{XL(30)}$ (Fig. 5b). We speculate that for the former gels the hollow particles more easily fragmented (due to low or negligible shell crosslinking) and involved less large-scale particle movement (*e.g.*, hollow particle-to-hollow particle bond breaking) under strain.
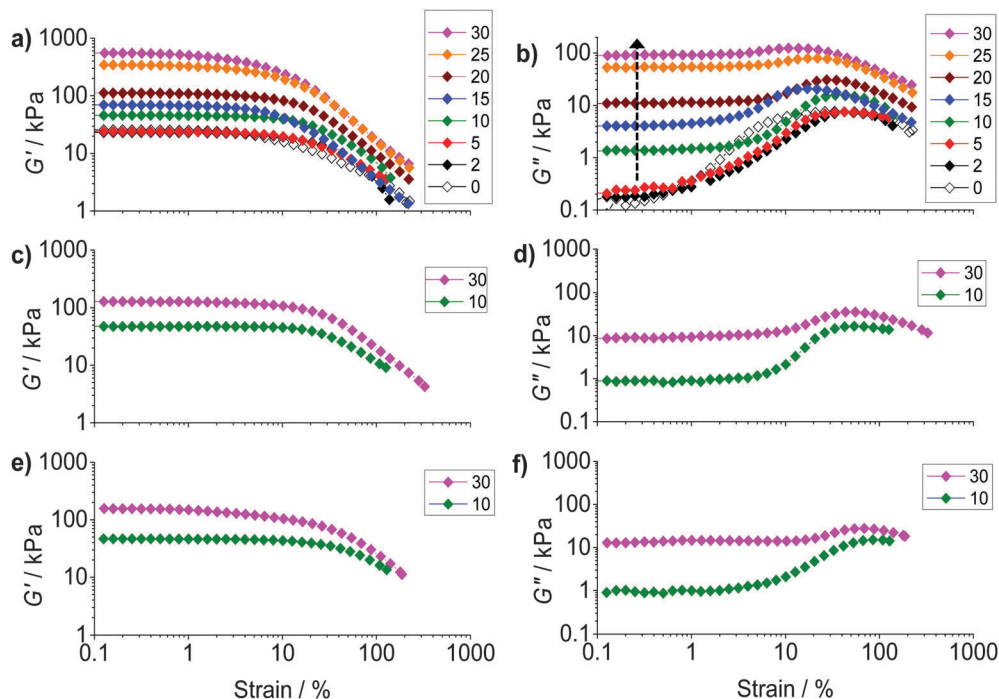
Fig. 5 Strain-sweep rheology study. Data for G' (left column) and G'' (right column) are shown as a function of strain for PAAm/HP$_{XL(y)}$ (a and b), PAAm/HP$_{VF(y)}$ (c and d) and PAAm/HP$_{(y)}$ (e and f). The values for y are shown in the legends. The arrow in (b) highlights the increase for G'' at low strain with increasing y.

To further probe dissipation within the composite gels the normalised loss modulus, $\Delta G_n''(=(G_{peak}'' - G_o'')/G_o'')$ was plotted (Fig. 6a). The values for G_{peak}'' and G_o'' are the maximum G'' value and the strain-independent value for G'' measured at low strain, respectively, obtained from the strain-sweep data (Fig. 5). This representation for the G'' data (which measures energy dissipated per unit strain) normalised the high strain energy loss (due to PAAm network breakdown) to that occurring at low strain (due to the hollow particles). It can be seen from Fig. 6a that the $\Delta G_n''$ values for PAAm/HP$_{XL(y)}$ decreased exponentially with increasing y. Such a pronounced change in relative energy loss is attributed to dissipative relaxation processes associated with the

percolated hollow particle network. For a percolated network it is reasonable to envisage that the proportion of inter-hollow particle contacts (and dissipative contacts) would increase very rapidly with increasing y.

The ductility of the composite gels was assessed from the critical strain (γ_{Crit}) which is the strain value at which $G' = G''$. The γ_{Crit} values were obtained from the data shown in Fig. 5 and are plotted as a function of y (Fig. 6b). Whilst there was scatter for the PAAm/HP$_{XL(y)}$ data it can be seen that the γ_{Crit} values increased for low values of y before decreasing at the highest y value (30%). Inclusion of HP$_{XL}$ was beneficial (or at the least was not detrimental) for composite gel ductility
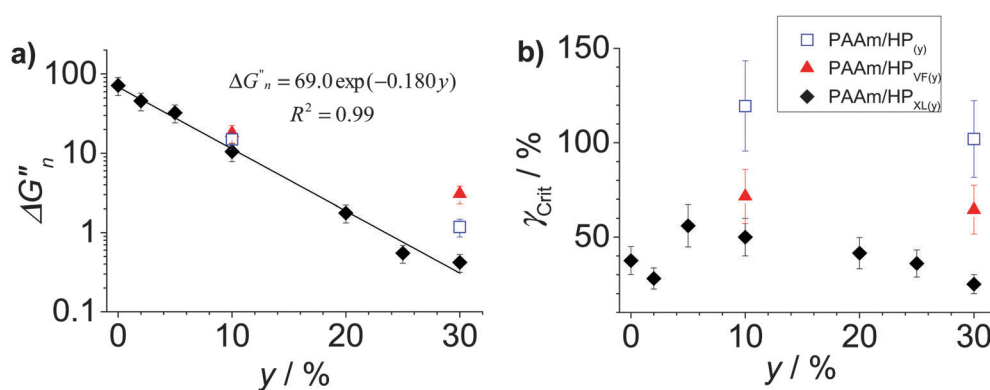

Fig. 6 Effects of particle concentration on gel dissipation and ductility. (a) Variation of $\Delta G_n''((=(G_{peak}'' - G_o'')/G_o'')$ where G_{peak}'' and G_o'' are maximum G'' and strain-independent G'' values, respectively) and (b) Variation of γ_{Crit} with particle concentration (y) for the composite gels. The data have been taken from Fig. 5.

compared to PAAm as judged by the γ_{Crit} values. Interestingly, inclusion of HP_{VF} and HP gave greater increases in composite gel ductility compared to HP_{XL}. We propose that the HP_{VF} and HP particles were less stiff (due to less or negligible intra-shell crosslinking) and were able to deform and/or fracture during strain. These inelastic processes dissipated fracture energy more uniformly, decreased crack propagation and increased overall composite gel ductility.

Effect of pH on the properties of PAAm/$HP_{XL(y)}$ gels

Hydrogels that contain pH-responsive hollow particles may have potential application for wound repair or membranes. In order to assess the effect of pH on the properties of PAAm/$HP_{XL(y)}$ composites we first investigated the response of the HP_{XL} particles to pH variation. Optical micrographs were obtained for HP_{XL} particles dispersed at pH values of 4.0

(Fig. 7a), 7.4 (Fig. 7b) and 12.3 (Fig. 7c). The hollow particles became noticeably more diffuse in appearance when the pH was greater than or equal to 7.4. The average size of the HP_{XL} particles at pH 4.0, 7.4 and 12.3 were 7.4 ± 4.1, 8.7 ± 3.4 and 11.2 ± 3.2 μm, respectively. Those values are consistent with pH-triggered hollow particle swelling. Importantly, the images shown in Fig. 7b and c show that shell crosslinking was effective in preventing dissolution of the hollow particles.

We next investigated the effects of pH on the morphology and mechanical properties of the PAAm/$HP_{XL(y)}$ gels. The pH values of 4.0 and 8.0 were selected in order to include the pH range for normal skin and a typical wound area.[54] Optical micrographs for the as-made PAAm/$HP_{XL(10)}$ gel (Fig. 8a) and CLSM images for the gels after swelling at pH values of 4.0 (Fig. 8b) and 8.0 (Fig. 8c) show that the hollow particles were present within the composite gels at both pH values. The hollow
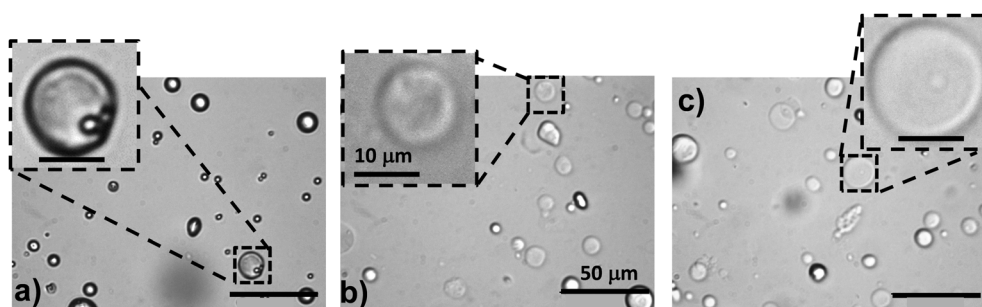

Fig. 7 Shell-crosslinked hollow particle morphologies at different pH values. Optical micrographs for HP_{XL} dispersions at pH values of (a) 4.0, (b) 7.4 and (c) 12.3. The scale bars in (b) also apply to (a) and (c).
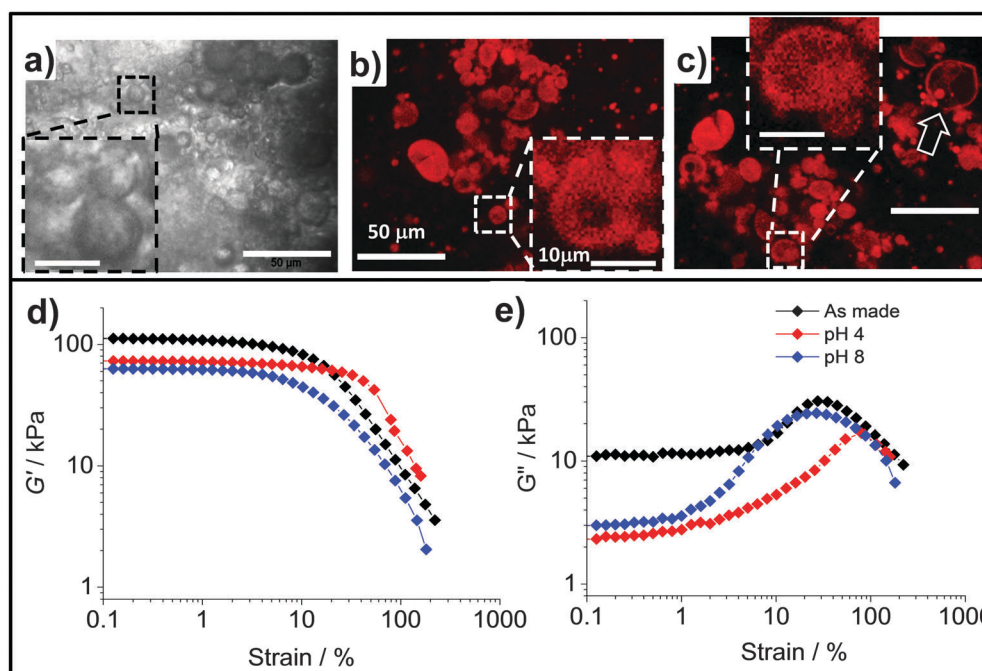

Fig. 8 Morphology and mechanical properties at different pH values. Optical microscopy (a) and CLSM images (b and c) for as-made (a) and PAAm/$HP_{XL(10)}$ gels at pH 4.0 (b) and 8.0 (c), respectively. The scale bars in (b) also apply to (a) and (c). The arrow in (c) highlights a large hollow particle. (d and e) Show strain-sweep rheology data for PAAm/$HP_{XL(20)}$ gels before and after swelling equilibrium at pH 4.0 and 8.0.

particles can be seen from the insets and also the arrow in Fig. 8c. There is also evidence of aggregates of hollow particles within the composite gels (Fig. 8b and c) which is consistent with the percolated morphology proposed in Scheme 2.

Strain-sweep rheology measurements were performed using PAAm/HP$_{XL(20)}$ gels which were swollen at pH 4.0 (degree of swelling, DS = 5.2 ± 0.2) and 8.0 (DS = 6.2 ± 0.1) and the data are shown in Fig. 8d and e. The initial DS for the as-made gel corresponds to 3.0. Consequently, swelling occurred at both pH values. A contribution to swelling originated from the osmotic pressure of the PAAm phase which became significant when the gels were no longer constrained by the limited amount of water used during their preparation. Compared to the modulus for the as-made gel, which had a G' value of ∼110 kPa (Fig. 8d), the G' values for the swollen gels decreased to 73 kPa (pH 4.0) and 63 kPa (pH 8.0), respectively. These decreases were due to increased swelling for the gels at both pH values. Taken together, both the DS and rheology data demonstrate stronger swelling for the gels at pH 8.0 and pH-responsiveness.

The values for γ_{Crit} determined from the strain-sweep data (Fig. 8d and e) obtained at pH 4.0 and 8.0 were 110 ± 22% and 30 ± 6.0%, respectively. The γ_{Crit} value at pH 8.0 (and hence ductility) had not significantly decreased compared to the as-made system (γ_{Crit} = 41.5 ± 8.3%) as a result of swelling. Whilst we currently do not have a simple explanation for the increased γ_{Crit} value at pH 4.0 the improved ductility compared to the as-made state is pleasing. These results show that the composite gels had good mechanical property robustness to swelling in the pH range of 4.0 to 8.0, which is potentially useful for membranes and wound healing applications.[55]

Conclusions

PAAm composite hydrogels containing micrometer-sized pH-responsive shell cross-linked hollow particles were prepared and studied for the first time. The hollow particles introduced here were vinyl functionalised and prepared by a scaleable method. A new finding for these particles was that the shell morphology became more uniform and spherical when the pH-responsive copolymer contained GMA. This result extends the range of functionalisation possibilities for this class of hollow particles[33] and should increase their versatility for future use. PAAm/HP$_{XL}$ composite gels were found to have tuneable mechanical properties that were governed by percolation. The percolated hollow particle network increased the modulus in a predictable manner and the ductility for all of the dispersions was at least as high (or better) than that for the parent PAAm gel. Control hollow particles showed that shell-crosslinking was important for obtaining the highest modulus improvement through hollow particle inclusion. The PAAm/HP$_{XL}$ composite gels were pH-responsive and showed increased swelling at pH 8.0 compared to pH 4.0. Because the composites have tuneable modulus values, good mechanical properties in the swollen state and are pH-responsive they may enable future applications as pH-responsive wound dressings or membranes.

References

1 N. A. Peppas, J. Z. Hilt, A. Khademhosseini and R. Langer, *Adv. Mater.*, 2006, **18**, 1345–1360.
2 N. A. Peppas, P. Bures, W. Leobandung and H. Ichikawa, *Eur. J. Pharm. Biopharm.*, 2000, **50**, 27–46.
3 D. Seliktar, *Science*, 2012, **336**, 1124–1128.
4 B. V Slaughter, S. S. Khurshid, O. Z. Fisher, A. Khademhosseini and N. A. Peppas, *Adv. Mater.*, 2009, **21**, 3307–3329.
5 A. A. Amini and L. S. Nair, *Biomed. Mater.*, 2012, **7**, 1–3.
6 J. P. Gong, Y. Katsuyama, T. Kurokawa and Y. Osada, *Adv. Mater.*, 2003, **15**, 1155–1158.
7 Y. Tanaka, R. Kuwabara, Y. H. Na, T. Kurokawa, J. P. Gong and Y. Osada, *J. Phys. Chem. B*, 2005, **109**, 11559–11562.
8 R. E. Webber, C. Creton, H. R. Brown and J. P. Gong, *Macromolecules*, 2007, **40**, 2919–2927.
9 K. Haraguchi, *Curr. Opin. Solid State Mater. Sci.*, 2007, **11**, 47–54.
10 K. Haraguchi, R. Farnworth, A. Ohbayashi and T. Takehisa, *Macromolecules*, 2003, **36**, 5732–5741.
11 K. Haraguchi and T. Takehisa, *Adv. Mater.*, 2002, **14**, 1120–1124.
12 K. Haraguchi, T. Takehisa and S. Fan, *Macromolecules*, 2002, **35**, 10162–10171.
13 S. Miyazaki, T. Karino, H. Endo, K. Haraguchi and M. Shibayama, *Macromolecules*, 2006, **39**, 8112–8120.
14 M. Shibayama, T. Karino, S. Miyazaki, S. Okabe, T. Takehisa and K. Haraguchi, *Macromolecules*, 2005, **38**, 10772–10781.
15 A. K. Gaharwar, N. A. Peppas and A. Khademhosseini, *Biotechnol. Bioeng.*, 2014, **111**, 441–453.
16 O. Okay and W. Oppermann, *Macromolecules*, 2007, **40**, 3378–3387.
17 Y. Xiang and D. Chen, *Eur. Polym. J.*, 2007, **43**, 4178–4187.
18 N. S. Satarkar and J. Z. Hilt, *J. Controlled Release*, 2008, **130**, 246–251.
19 H. Bai, C. Li, X. Wang and S. Gaoquan, *Chem. Commun.*, 2010, **46**, 2376–2378.
20 Z. Cui, A. H. Milani, P. J. Greensmith, J. Yan, D. J. Adlam, J. A. Hoyland, I. A. Kinloch, A. J. Freemont and B. R. Saunders, *Langmuir*, 2014, **30**, 13384–13393.
21 S. R. Shin, S. M. Jung, M. Zalabany, K. Kim, P. Zorlutuna, S. B. Kim, M. Nikkhah, M. Khabiry, M. Azize, J. Kong, K.-T. Wan, T. Palacios, M. R. Dokmeci, H. Bae, X. S. Tang and A. Khademhosseini, *ACS Nano*, 2013, **7**, 2369–2380.
22 T. H. Tran, A. Vimalanandan, G. Genchev, J. Fickert, K. Landfester, D. Crespy and M. Rohwerder, *Adv. Mater.*, 2015, **27**, 3825–3830.
23 L. H. Lim, A. Tan, S. Simovic and C. A. Prestidge, *Int. J. Pharm.*, 2011, **409**, 297–306.
24 S. H. Im, T. Herricks, Y. T. Lee and Y. Xia, *Nat. Mater.*, 2005, **4**, 671–675.

25 G. Sukhorukov, A. Fery and H. Mohwald, *Prog. Polym. Sci.*, 2005, **30**, 885–897.

26 O. J. Cayre and S. Biggs, *J. Mater. Chem.*, 2009, **19**, 2724–2728.

27 M. Sauer and W. Meier, *Chem. Commun.*, 2001, 55–56.

28 H. N. Yow and A. F. Routh, *Soft Matter*, 2006, **2**, 940–949.

29 I. Choi, S. T. Malak, W. Xu, W. T. Heller, C. Tsitsilianis and V. V. Tsukruk, *Macromolecules*, 2013, **46**, 1425–1436.

30 W. Xu, P. A. Ledin, F. A. Plamper, C. V. Synatschke, A. H. E. Müller and V. V. Tsukruk, *Macromolecules*, 2014, **47**, 7858–7868.

31 A. Zelikin, Q. Li and F. Caruso, *Chem. Mater.*, 2008, **20**, 2655–2661.

32 F. Caruso, R. A. Caruso and H. Mohwald, *Science*, 1998, **282**, 1111–1114.

33 R. Bird, T. J. Freemont and B. R. Saunders, *Chem. Commun.*, 2011, **47**, 1443–1445.

34 S. Nayak, D. Gan, M. J. Serpe and L. A. Lyon, *Small*, 2005, **4**, 416–421.

35 R. Contreras-Cáceres, L. Schellkopf, C. Fernández-López, I. Pastoriza-Santos, J. Pérez-Juste and M. Stamm, *Langmuir*, 2015, **31**, 1142–1149.

36 F. Zhang and C.-C. Wang, *Colloid Polym. Sci.*, 2008, **286**, 889–895.

37 S. S. Halacheva, D. J. Adlam, T. J. Freemont, J. Hoyland and B. R. Saunders, *Biomacromolecules*, 2014, **15**, 1814–1827.

38 S. S. Halacheva, T. J. Freemont and B. S. Saunders, *J. Mater. Chem. B*, 2013, **1**, 4035–4036.

39 R. Bird, T. Freemont and B. R. Saunders, *Soft Matter*, 2012, **8**, 1047–1057.

40 R. Bird, S. Tungchaiwattana, T. Freemont and B. R. Saunders, *Soft Matter*, 2012, **8**, 3062.

41 G. B. Trappmann, J. E. Connelly, D. G. T. Strange, Y. Li, M. L. Oyen, M. A. Cohen Stuart, H. Boehm, B. Li, V. Vogel, J. P. Spatz, F. M. Watt and W. T. S. Huck, *Nat. Mater.*, 2012, **11**, 642–649.

42 J. R. Capadona, K. Shanmuganathan, S. Trittschuh, S. Seidel, S. J. Rowan and C. Weder, *Biomacromolecules*, 2009, **10**, 712–716.

43 L. Carlsson, S. Rose, D. Hourdet and A. Marcellan, *Soft Matter*, 2010, **6**, 3619–3631.

44 H. H. Winter and F. Chambon, *J. Rheol.*, 1986, **30**, 367–382.

45 S. Rose, A. Dizeux, T. Narita, D. Hourdet and A. Marcellan, *Macromolecules*, 2013, **46**, 4095–4104.

46 R. Perez-Aparicio, A. Vieyres, P.-A. Albouy, O. Sanseau, L. Vanel, D. R. Long and P. Sotta, *Macromolecules*, 2013, **46**, 8694–8972.

47 A. D. Drozdov, *Compos. Interfaces*, 2013, **20**, 673–692.

48 W.-C. Lin, W. Fan, A. Marcellan, D. Hourdet and C. Creton, *Macromolecules*, 2010, **43**, 2554–2563.

49 A. Delalleau, G. Josse, J. M. Lagarde, H. Zahouani and J. M. Bergheau, *Wear*, 2008, **264**, 405–410.

50 G. C. Engelmayr, M. Cheng, C. J. Bettinger, J. T. Borenstein, R. Langer and L. E. Freed, *Nat. Mater.*, 2008, **7**, 1003–1010.

51 E. van der Linden and L. M. C. Sagis, *Langmuir*, 2001, **17**, 5821–5824.

52 T. Mitsumata, Y. Kosugi and S. Ouchi, *Prog. Colloid Polym. Sci.*, 2009, **136**, 163–170.

53 M. C. Grant and W. B. Russel, *Phys. Rev. E: Stat. Phys., Plasmas, Fluids, Relat. Interdiscip. Top.*, 1993, **47**, 2606.

54 S.-T. Oh, W.-R. Kim, S.-H. Kim, Y.-C. Chung and J.-S. Park, *Fibers Polym.*, 2011, **12**, 159–165.

55 A. M. Diez-Pascual and A. L. Diez-Vicente, *Biomacromolecules*, 2015, **16**, 2631–2644.